Supplementary Material for *mpcGear: Multi-Point Conjugation Gear Mechanisms*

This supplementary material is composed of seven parts. First, we present the derivation of our measure of dynamic form closure (see Section 4.2 of the paper). Second, we give the explicit expressions for the energy terms used to model one tooth pair (see Section 5.1). Third, we present the explicit energy formulations for modeling one sub-gear pair (see Section 5.2). Fourth, we specify the constraints used to model K sub-gear pairs (see Section 5.3.1). Fifth, we describe the details of our optimization solver (see Section 5.3.2). Sixth, we detail the procedure for finalizing the modeling of a complete mpcGear (see Section 5.4). Finally, we provide a discussion about how different numbers of driver and follower teeth restrict the feasible design space. In addition, Table 1 summarizes the statistics of all results presented in this paper.

1 Measure of Dynamic Form Closure

In this section, inspired by the analysis of optimal form-closure grasps in [Cornellà and Suárez 2009], we derive our measure of dynamic form closure for mechanisms with multi-point conjugation. We first review the dynamic form closure condition in the paper:

$$U \subset \bigcup_{1 \leqslant k \leqslant K} U_k(t), \quad \forall t \in [0, T), \tag{1}$$

where U is the infinitesimal N-DOF motion space of the follower surface, and $U_k(t)$ is the set of infinitesimal rigid motions of the follower surface restrained by the conjugation point $\mathbf{p}_k(t)$ with normal $\mathbf{n}_k(t)$ at time t. According to [Chen et al. 2024], this condition is equivalent to

$$\mathbf{0} \in \text{interior}\left(\text{conv}(\{\tilde{\mathbf{n}}_k(t)\}_{1 \leqslant k \leqslant K})\right), \quad \forall t \in [0, T), \tag{2}$$

where $\tilde{\mathbf{n}}_k(t)$ is the normalized projection of the generalized normal $\hat{\mathbf{n}}_k(t)$ onto span(U) (the linear subspace spanned by the motion space U), conv($\cdot$) denotes the convex hull of a set of points, and interior($\cdot$) is the interior operator taken within span(U). In other words, Equation (2) requires that the zero vector $\mathbf{0}$ lies in the relative interior of conv($\{\tilde{\mathbf{n}}_k(t)\}$). In the following derivations, all interior and boundary operations are also taken within span(U).

We now proceed to derive the measure of dynamic form closure. At time t, we assume that the magnitude of the force $\mathbf{f}_k(t)$ exerted by the driver surface at the k-th conjugation point $\mathbf{p}_k(t)$ with contact normal $\mathbf{n}_k(t)$ is a non-negative number $a_k(t)$, $1 \leqslant k \leqslant K$. The force $\mathbf{f}_k(t) = a_k(t)\mathbf{n}_k(t)$ produces a torque with respect to the center of the follower surface, chosen as the origin, given by $\boldsymbol{\tau}_k(t) = \mathbf{p}_k(t) \times a_k(t)\mathbf{n}_k(t)$. The components of the force and torque constitute the wrench vector:

$$\mathbf{w}_k(t) = \begin{bmatrix} \mathbf{f}_k(t) \\ \boldsymbol{\tau}_k(t) \end{bmatrix} = \begin{bmatrix} a_k(t)\mathbf{n}_k(t) \\ \mathbf{p}_k(t) \times a_k(t)\mathbf{n}_k(t) \end{bmatrix}, \tag{3}$$

from which it is evident that $\mathbf{w}_k(t) = a_k(t)\hat{\mathbf{n}}_k(t)$. Since the set of all possible infinitesimal motions of the follower surface is denoted by U, we only consider the component of $\mathbf{w}_k(t)$ within the span(U). Accordingly, we denote the projections of $\mathbf{w}_k(t)$ and $\hat{\mathbf{n}}_k(t)$ onto span(U) as $\overline{\mathbf{w}}_k(t)$ and $\overline{\mathbf{n}}_k(t)$ respectively under Equation (3) in the paper. Here, $\overline{\mathbf{w}}_k(t)$ is referred to as the effective wrench. Note that $\tilde{\mathbf{n}}_k(t)$ is the unit vector of $\overline{\mathbf{n}}_k(t)$. We consider that the force exerted by the driver surface is limited to $a_{\max}$ owing to a maximum available power for the actuator. Then all the attainable effective wrenches applied to the follower surface form a set:

$$\mathcal{W}(t) = \left\{ \sum_{k=1}^{K} \overline{\mathbf{w}}_k(t) \;\middle|\; \begin{array}{l} \overline{\mathbf{w}}_k(t) = a_k(t)\overline{\mathbf{n}}_k(t), \\ a_k(t) \geqslant 0, \quad \sum_{k=1}^{K} a_k(t) \leqslant a_{\max} \end{array} \right\}. \tag{4}$$

Without loss of generality, we assume $a_{\max} = 1$. Now we prove that the dynamic form closure condition in Equation (2) is equivalent to

$$\mathbf{0} \in \text{interior}\left(\text{conv}(\{\overline{\mathbf{n}}_k(t)\}_{1 \leqslant k \leqslant K})\right), \quad \forall t \in [0, T). \tag{5}$$

Proof. For a fixed t, denote $u_k = \tilde{\mathbf{n}}_k(t)$ and $v_k = \overline{\mathbf{n}}_k(t)$, $1 \leqslant k \leqslant K$. Let $\alpha_k = \|v_k\| > 0$, so $v_k = \alpha_k u_k$.

($\Rightarrow$) Assume $\mathbf{0} \in$ interior(conv($\{u_k\}$)). There exist coefficients $\lambda_k > 0$, $1 \leqslant k \leqslant K$, with $\sum_{k=1}^{K} \lambda_k = 1$ and $\sum_{k=1}^{K} \lambda_k u_k = \mathbf{0}$. Define

$$\mu_k = \frac{\lambda_k / \alpha_k}{\sum_{i=1}^{K} \lambda_i / \alpha_i}. \tag{6}$$

Then $\mu_k > 0$ and $\sum_{k=1}^{K} \mu_k = 1$, and

$$\sum_{k=1}^{K} \mu_k v_k = \sum_{k=1}^{K} \mu_k \alpha_k u_k = \frac{1}{\sum_{i=1}^{K} \lambda_i / \alpha_i} \sum_{k=1}^{K} \lambda_k u_k = \mathbf{0}, \tag{7}$$

which yields $\mathbf{0} \in$ interior(conv($\{v_k\}$)).

($\Leftarrow$) Conversely, assume $\mathbf{0} \in$ interior(conv($\{v_k\}$)). Then there exist coefficients $\mu_k > 0$, $1 \leqslant k \leqslant K$, with $\sum_{k=1}^{K} \mu_k = 1$ and $\sum_{k=1}^{K} \mu_k v_k = \mathbf{0}$. Define

$$\lambda_k = \frac{\mu_k \alpha_k}{\sum_{i=1}^{K} \mu_i \alpha_i}. \tag{8}$$

Table 1. Statistics of the results in the paper. From left to right, the columns correspond to the mpcGear class, the number of sub-gear pairs (K), the energy terms $E_{\text{validTime}}$ and E_{minMsr}, and the optimization time required to model K sub-gear pairs.

Figure(s)	mpcGear class	# sub-gear pairs (K)	$E_{\text{validTime}}$	E_{minMsr}	Optim. time (min)
1	3R	4	1.0	4.270	44.63
2	3R	4	1.0	2.844	58.59
7	3R	4	1.0	2.624	42.07
9	1R	2	1.0	10.626	16.52
	1R1T	3	1.0	0.080	32.78
	3R	4	1.0	1.565	45.11
	3R1T	6	1.0	0.217	147.61
10 & 12	3R	4	1.0	2.887	56.57
13	3R	4	1.0	4.158	45.78

Again, $\lambda_k > 0$ and $\sum_{k=1}^{K} \lambda_k = 1$, and

$$\sum_{k=1}^{K} \lambda_k u_k = \sum_{k=1}^{K} \lambda_k \frac{v_k}{\alpha_k} = \frac{1}{\sum_{i=1}^{K} \mu_i \alpha_i} \sum_{k=1}^{K} \mu_k v_k = \mathbf{0}, \tag{9}$$

which yields $\mathbf{0} \in \text{interior}(\text{conv}(\{u_k\}))$. □

Next, we prove that under the equivalent dynamic form closure condition in Equation (5), $\mathcal{W}(t)$ satisfies

$$\mathcal{W}(t) = \text{conv}\left(\{\overline{\mathbf{n}}_k(t)\}_{1 \leqslant k \leqslant K}\right). \tag{10}$$

Proof. Fix t and denote $\mathcal{N}(t) = \{\overline{\mathbf{n}}_k(t)\}_{1 \leqslant k \leqslant K}$. $\text{conv}(\mathcal{N}(t)) \subseteq \mathcal{W}(t)$ is trivial by definition. From (5), we have in particular $\mathbf{0} \in \text{conv}(\mathcal{N}(t))$. Next, we prove $\mathcal{W}(t) \subseteq \text{conv}(\mathcal{N}(t))$.

Take any $\mathbf{y} \in \mathcal{W}(t)$. Then $\mathbf{y} = \sum_{k=1}^{K} a_k \overline{\mathbf{n}}_k(t)$ with $a_k \geqslant 0$ and $s = \sum_{k=1}^{K} a_k \leqslant 1$. If $s = 0$, then $\mathbf{y} = \mathbf{0} \in \text{conv}(\mathcal{N}(t))$. If $s > 0$, define $\lambda_k = a_k / s$, so that $\lambda_k \geqslant 0$ and $\sum_{k=1}^{K} \lambda_k = 1$. Then

$$\mathbf{y} = s \sum_{k=1}^{K} \lambda_k \overline{\mathbf{n}}_k(t), \text{ with } \mathbf{x} = \sum_{k=1}^{K} \lambda_k \overline{\mathbf{n}}_k(t) \in \text{conv}(\mathcal{N}(t)). \tag{11}$$

Using $\mathbf{0} \in \text{conv}(\mathcal{N}(t))$ and convexity, we have

$$\mathbf{y} = (1 - s)\mathbf{0} + s\mathbf{x} \in \text{conv}(\mathcal{N}(t)). \tag{12}$$

Therefore $\mathcal{W}(t) \subseteq \text{conv}(\mathcal{N}(t))$. □

By Equations (5) and (10), we know that for a mechanism with multi-point conjugation satisfying the dynamic form closure condition, the interior of $\mathcal{W}(t)$ contains $\mathbf{0}$:

$$\mathbf{0} \in \text{interior}\left(\mathcal{W}(t)\right), \quad \forall t \in [0, T). \tag{13}$$

See Figure 3(b) in the paper. To quantify the ability to resist arbitrary external loads, we follow [Cornellà and Suárez 2009] and define our measure as the worst-case attainable effective wrench magnitude over all directions in the motion space U; namely, for each direction in U, we consider the maximum attainable effective wrench magnitude, and then take the minimum over all directions:

$$Q(t) = \min_{\mathbf{u} \in U} \max_{\substack{\lambda \mathbf{u} \in \mathcal{W}(t) \\ \lambda > 0}} \lambda. \tag{14}$$

However, this definition of the measure is not intuitive. Note that the motion space U of a follower-support joint used in practice is typically an entire unit hypersphere. For example, U of a spherical joint is a 2-sphere. According to Equations (10) and (13), we can reformulate Equation (14) as

$$Q(t) = -\,\text{dist}(\mathbf{0}, \partial\mathcal{W}(t)) = -\,\text{dist}(\mathbf{0}, \partial\,\text{conv}(\{\overline{\mathbf{n}}_k(t)\}_{1 \leqslant k \leqslant K})), \tag{15}$$

where $\text{dist}(\cdot, \cdot)$ denotes the signed distance operator, taken as negative inside $\mathcal{W}(t)$, and ∂ denotes the boundary operator, taken relative to $\text{span}(U)$.

This reformulation shows that $Q(t) > 0, \forall t \in [0, T)$ holds if and only if the interior of $\text{conv}(\{\overline{\mathbf{n}}_k(t)\}_{1 \leqslant k \leqslant K})$ contains $\mathbf{0}$, which is also equivalent to Equation (5). Given the equivalence between Equations (5) and (2), the dynamic form closure condition is ensured. Therefore, the dynamic form closure condition in Equation (2) can be reformulated as

$$Q(t) > 0, \quad \forall t \in [0, T). \tag{16}$$

Furthermore, a larger value of $Q(t)$ indicates better load-bearing performance of the mechanism. In other words, we use the Euclidean distance from the zero vector $\mathbf{0}$ to the boundary of the convex hull of $\{\overline{\mathbf{n}}_k(t)\}_{1 \leqslant k \leqslant K}$ to measure the quality of dynamic form closure of a multi-point conjugation mechanism.

2 Energy Terms for Modeling One Tooth Pair

In Section 5.1 of the paper, we need to enforce $\mathbf{n}_{k,j}(t) \perp \mathbf{T}^1_{k,j}(t)$ at any time $t \in (t^s_{k,j}, t^e_{k,j})$. Thus, we introduce an energy term E_{norm} defined as

$$E_{\text{norm}} = \sum_{i=0}^{I} \left(\mathbf{n}_{k,j}(t_{k,j,i}) \cdot \frac{\mathbf{T}^1_{k,j}(t_{k,j,i})}{\|\mathbf{T}^1_{k,j}(t_{k,j,i})\|} \right)^2, \tag{17}$$

over $I + 1$ uniform samples $t_{k,j,i} = (1 - i/I)\, t^s_{k,j} + (i/I)\, t^e_{k,j}$, $0 \leqslant i \leqslant I$.

In addition to the basic requirements for point conjugation, we introduce two additional energy terms to facilitate practical fabrication. First, we require the tangents of the pair of open 3D conjugate curves at the conjugation point $\mathbf{p}_{k,j}(t)$ to be nearly collinear:

$$E_{\text{tang}} = \sum_{i=0}^{I} \left\| \frac{\mathbf{T}^1_{k,j}(t_{k,j,i})}{\|\mathbf{T}^1_{k,j}(t_{k,j,i})\|} - \frac{\mathbf{T}^2_{k,j}(t_{k,j,i})}{\|\mathbf{T}^2_{k,j}(t_{k,j,i})\|} \right\|^2; \tag{18}$$

Second, we require the two open 3D conjugate curves to be approximately coplanar:

$$E_{\text{plan}} = \sum_{\alpha} \sum_{i=0}^{I} \left\| (-1)^{\alpha} \mathbf{n}_{k,j}(t_{k,j,i}) - \frac{\boldsymbol{\kappa}^{\alpha}_{k,j}(t_{k,j,i})}{\|\boldsymbol{\kappa}^{\alpha}_{k,j}(t_{k,j,i})\|} \right\|^2, \tag{19}$$

where $\boldsymbol{\kappa}^{\alpha}_{k,j}(t)$ denotes the curvature vector of the α-th curve at the conjugation point $\mathbf{p}_{k,j}(t)$, for $\alpha \in \{1, 2\}$.

3 Additional Geometric Requirements for Modeling a Sub-Gear Pair

In Section 5.2 of the paper, when modeling J tooth pairs as a sub-gear pair, we aim to achieve a well-structured layout of the J tooth pairs in the global frame to facilitate fabrication. To this end, we introduce two additional energy terms and two constraints. First, we aim to arrange these tooth pairs in a compact manner, similar to the arrangement in a traditional gear, such that for each $\alpha \in \{1, 2\}$, the sets of start points and end points of 3D conjugate curves $\mathbf{p}^{\alpha}_{k,j}(t)$ each lie close to a circle:

$$E_{\text{circ}} = \sum_{\alpha} \sum_{j=1}^{J} \left(\left\| \Delta_j \mathbf{b}^{\alpha,s}_{k,j} \right\|^2 + \left\| \Delta_j \mathbf{b}^{\alpha,e}_{k,j} \right\|^2 \right), \tag{20}$$

where $\mathbf{b}^{\alpha,\chi}_{k,j} = \mathbf{p}^{\alpha}_{k,j}(t^{\chi}_{k,j})$ denotes the start or end point of the curve $\mathbf{p}^{\alpha}_{k,j}(t)$ for $\chi = s$ or $\chi = e$, respectively, and Δ_j is the discrete second-difference operator with respect to the cyclic index j: $\Delta_j \mathbf{x}_j = \mathbf{x}_{j+1} - 2\mathbf{x}_j + \mathbf{x}_{j-1}$. The index j is interpreted cyclically, i.e., $j = J$ is followed by $j = 1$; the same applies hereafter. Second, to ensure sufficient spacing between consecutive open 3D conjugate curves on both the follower and driver surfaces, we propose a constraint that enforces a lower bound d on the distance between consecutive start points

and between consecutive end points:

$$C_{\text{spac}} = d - \left\| \mathbf{b}_{k,j+1}^{\alpha,\chi} - \mathbf{b}_{k,j}^{\alpha,\chi} \right\| \leqslant 0 \,, \tag{21}$$

for $\alpha \in \{1,2\}$, $\chi \in \{s,e\}$, $1 \leqslant j \leqslant J$. In our experiments, $d = 2.5$. Third, we introduce an energy term to encourage the circles formed by the start points and the end points to be nearly parallel:

$$E_{\text{para}} = \sum_{\alpha} \left\| \frac{\mathbf{n}_k^{\alpha,s}}{\|\mathbf{n}_k^{\alpha,s}\|} - \frac{\mathbf{n}_k^{\alpha,e}}{\|\mathbf{n}_k^{\alpha,e}\|} \right\|^2 , \tag{22}$$

where $\mathbf{n}_k^{\alpha,\chi} = \sum_{1 \leqslant j \leqslant J} \left(\mathbf{b}_{k,j+1}^{\alpha,\chi} - \mathbf{c}_k^{\alpha,\chi}\right) \times \left(\mathbf{b}_{k,j}^{\alpha,\chi} - \mathbf{c}_k^{\alpha,\chi}\right)$ can be regarded as the approximate normal vector of the plane fitted to the circle formed by $\{\mathbf{b}_{k,j}^{\alpha,\chi}\}$, and $\mathbf{c}_k^{\alpha,\chi} = \frac{1}{J} \sum_{1 \leqslant j \leqslant J} \mathbf{b}_{k,j}^{\alpha,\chi}$ is the centroid of $\{\mathbf{b}_{k,j}^{\alpha,\chi}\}$, $\chi \in \{s,e\}$. Fourth, to guarantee separation along the normal direction of the planes containing the two circles formed by the start points and the end points, we require the projection of the difference vector between the two centroids of $\{\mathbf{b}_{k,j}^{2,s}\}$ and $\{\mathbf{b}_{k,j}^{2,e}\}$ onto the direction $\mathbf{n}_k^{2,s}$ to be at least w:

$$C_{\text{widt}} = w - (-1)^{\mu} \left(\mathbf{c}_k^{2,s} - \mathbf{c}_k^{2,e}\right) \cdot \frac{\mathbf{n}_k^{2,s}}{\|\mathbf{n}_k^{2,s}\|} \leqslant 0 \,, \tag{23}$$

where the factor $(-1)^{\mu}$, $\mu \in \{1,2\}$, allows either ordering of the two centroids along the normal direction $\mathbf{n}_k^{2,s}$, facilitating the generation of diverse sub-gear pairs during the subsequent optimization. In our experiments, $w = 9.0$.

4 Constraints for Modeling K Sub-Gear Pairs

In Section 5.3 of the paper, we have two constraints similar to those in [Chen et al. 2024] for the optimization of the K sub-gear pairs. The first constraint is to satisfy Equation (3) in the paper, preventing $\overline{\mathbf{n}}_k(t)$ from becoming $\mathbf{0}$:

$$C_{\text{closure}} = C(\mathbf{n}_{k,j}(t), \mathbf{p}_{k,j}(t), U) \leqslant 0, \quad \forall k, j, \forall t \in (t_{k,j}^s, t_{k,j}^e). \tag{24}$$

For example, the above constraint is equivalent to avoiding $\mathbf{n}_{k,j}(t) \times \mathbf{p}_{k,j}(t) = 0$ for mpcGear_3R, so the expression can be written as:

$$C_{\text{closure}} = \left(\mathbf{n}_{k,j}(t) \cdot \frac{\mathbf{p}_{k,j}(t)}{\|\mathbf{p}_{k,j}(t)\|} \right)^2 - \cos^2(\gamma_0 + \frac{\pi}{2}), \tag{25}$$

where γ_0 is a threshold set as 60° in our experiments. In our experiments, we use the same C_{closure} for mpcGear_3R1T with $\gamma_0 = 80^\circ$. We apply a similar treatment of C_{closure} to mpcGear_1R and mpcGear_1R1T. The corresponding expressions can be derived analogously, and related formulations can be found in [Chen et al. 2024].

The second constraint aims to prevent interference among the K sub-gear pairs. We require that the start points and end points of $\mathbf{p}_{k,j}^2(t)$ are constrained to lie within disjoint, equal-length intervals along the z axis:

$$z_k^{\min} \leqslant \mathbf{b}_{k,j}^{2,\chi}.z \leqslant z_k^{\max}, \quad \forall k, j, \chi, \tag{26}$$

where $\mathbf{b}_{k,j}^{2,\chi}.z$ is the z-coordinate of $\mathbf{b}_{k,j}^{2,\chi}$.

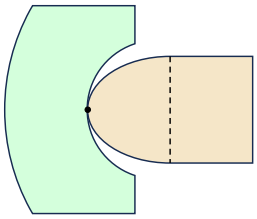

Fig. 1. A selected pair of cross-sections used to sweep the driver and follower tooth surfaces.

5 Optimization Solver for Modeling K Sub-Gear Pairs

We solve the optimization problem using a strategy similar to that in [Chen et al. 2024]. For a given K, we first solve for $\{\mathcal{P}_k\}_{1 \leqslant k \leqslant K}$ and $\{\vartheta_k\}_{1 \leqslant k \leqslant K}$ using a two-stage approach:

(1) *Candidate generation.* A candidate of the K sub-gear pairs can be generated by solving the optimization in Equation (10) in the paper incorporating the two constraints in Equations (24) and (26) and an additional energy term to promote diversity:

$$E_{\text{vary}} = \sum_{j=1}^{J} \sum_{i=0}^{I} \left\| \frac{\overline{\mathbf{n}}_{k,j}(t_{k,j,i})}{\|\overline{\mathbf{n}}_{k,j}(t_{k,j,i})\|} - \mathbf{u} \right\|^2 , \mathbf{u} \in \mathcal{U}, \tag{27}$$

where $\mathcal{U}$ is a set uniformly sampled from the motion set U. This term is added to the optimization in Equation (10) in the paper with a weight of 1.0. For each $\mu \in \{1,2\}$ and each $\mathbf{u} \in \mathcal{U}$, we solve the optimization problem for each $1 \leqslant k \leqslant K$ to obtain a candidate of K sub-gear pairs.

(2) *Selection.* We utilize a genetic algorithm to combine these candidates to obtain the final K sub-gear pairs with the optimal measure of dynamic form closure. An individual $\mathbf{I}_m$ is considered better than another individual $\mathbf{I}_n$ if one of the following conditions is satisfied:
   (a) $E_{\text{validTime}}(\mathbf{I}_m) > E_{\text{validTime}}(\mathbf{I}_n)$,
   (b) $E_{\text{validTime}}(\mathbf{I}_m) = E_{\text{validTime}}(\mathbf{I}_n)$ & $E_{\text{minMsr}}(\mathbf{I}_m) > E_{\text{minMsr}}(\mathbf{I}_n)$.

According to Equation (2) in the paper, at least $N+1$ sub-gear pairs are necessary to generate a motion in N-DOF motion space. To obtain a compact mechanism, the number of sub-gear pairs, K, should be as small as possible. Hence, we start by trying to find a solution with $K = N + 1$ sub-gear pairs using the above algorithm. If we cannot find such a solution satisfying the dynamic form closure condition, we increase K by one until we find a feasible solution.

6 Modeling Multi-Point Conjugation Gear Mechanisms

Modeling a multi-point conjugation joint. After the optimization, we obtain the optimized control points $\{\{\mathcal{P}_k\}, \{\vartheta_k\}\}$. We then obtain the open 3D conjugate curves $\{\mathbf{p}_{k,j}^{\alpha}(t)\}$ and normals $\{\mathbf{n}_{k,j}^{\alpha}(t)\}$ using Equations (5) and (6) in the paper. Following [Chen et al. 2024], we model the shape of each tooth on the follower gear by sweeping a cross-section formed by a semi-ellipse joined to a rectangle along $\mathbf{p}_{k,j}^2(t)$ and aligning the major axis of the ellipse with $\mathbf{n}_{k,j}^2(t)$; see Figure 1. The tooth shape of the driver gear is initially modeled using a similar sweeping strategy, with a C-like cross-section consisting of elliptical arcs and straight-line segments. These teeth

on the driver gear are then carved progressively using the teeth on the follower gear by simulating their conjugate motions for a whole period $[0, T)$ to ensure collision-free conjugate motion. This carving method guarantees that the conjugate surface pair $\mathbf{S}^1$ and $\mathbf{S}^2$ satisfies the induced normal curvature condition in [Chen et al. 2024] at each conjugation point. All the teeth on the gears form a multi-point conjugation joint.

Modeling the driver gear and the follower gear. After modeling the teeth as a multi-point conjugation joint, we model the driver gear as well as the follower gear by connecting their respective sets of teeth into unified bodies. We take the follower gear as an example. First, we model a central hub as the primary body of the gear. This central hub is a swept surface, where a circular profile serves as the cross-section and the guide curve is a B-spline modeled by Hermite interpolation. It not only passes through the centroids $\{\mathbf{c}_k^{2,\chi}\}$ but also aligns its tangents with the corresponding normals $\{\mathbf{n}_k^{2,\chi}\}$. Second, we model spokes $\{\mathbf{s}_{k,j}\}$ to connect the teeth and the central hub. We model the spoke $\mathbf{s}_{k,j}$ of a tooth $\mathbf{t}_{k,j}$ using the convex hull of the points on the back face of the tooth and a cylinder whose end-face centers are at $\mathbf{c}_k^{2,s}$ and $\mathbf{c}_k^{2,e}$. Finally, the follower gear is modeled by taking the union of all the teeth, spokes, and the central hub.

Finalization of modeling a mpcGear. Given the geometry of both gears, we add the driver-support joint and follower-support joint, and model a support using several pillars and a base plate to hold the gears. In order to add a follower-support joint for mpcGear_3R and mpcGear_3R1T, we need to carve the central hub to form a sphere in the middle as the sphere of the spherical joint.

7 Limitations under Unequal Numbers of Teeth

Our current formulation is limited when handling unequal numbers of driver and follower teeth. In all results in this paper, both the driver and the follower use $J = 10$ teeth, leading to a periodic one-to-one tooth correspondence.

Failure may arise even when the number of driver teeth is an integer multiple of that of the follower but the two numbers are unequal. Figure 14(c) in the paper shows such an example, where the driver and follower have 12 and 6 teeth, respectively, and the follower completes two motion periods while the driver completes one. As a result, the driver rotates more slowly, and the modeled driver teeth tend to be longer and are more likely to collide with non-corresponding follower teeth.

The situation becomes even more restrictive when the number of driver teeth is not an integer multiple of that of the follower. In this case, a single driver tooth must mesh with at least two follower teeth. Under our modeling framework, this would require these follower teeth to share the same locus curve $\mathbf{p}_{k,j}(t)$ and contact normal $\mathbf{n}_{k,j}(t)$. However, because the follower motion is user-specified, different follower teeth generally have different kinematics, so such a common locus curve and contact normal do not necessarily exist. Consequently, the design space becomes highly restricted, and only very special motions, such as uniform 1-DOF rotations, remain feasible for generation.

References

Ke Chen, Siqi Li, Peng Song, Jianmin Zheng, and Ligang Liu. 2024. mpcMech: Multi-Point Conjugation Mechanisms. *ACM Transactions on Graphics (SIGGRAPH Asia)* 43, 6 (2024), 211:1–211:14.

Jordi Cornellà and Raúl Suárez. 2009. Efficient Determination of Four-point Form-closure Optimal Constraints of Polygonal Objects. *IEEE Transactions on Automation Science and Engineering* 6, 1 (2009), 121–130.